Title

A Novel Bioengineered miR-127 Prodrug Suppresses the Growth and Metastatic Potential of Triple-Negative Breast Cancer Cells

Journal

Cancer Research, 80(3)

ISSN

0008-5472

Authors

Umeh-Garcia, Maxine
Simion, Catalina
Ho, Pui-Yan
et al.

Publication Date

2020-02-01

DOI

10.1158/0008-5472.can-19-0656

Peer reviewed

HHS Public Access

Author manuscript

Cancer Res. Author manuscript; available in PMC 2020 August 01.

Published in final edited form as:

Cancer Res. 2020 February 01; 80(3): 418–429. doi:10.1158/0008-5472.CAN-19-0656.

A Novel Bioengineered MicroRNA-127 Prodrug Suppresses The Growth And Metastatic Potential Of Triple Negative Breast Cancer Cells

Maxine Umeh-Garcia[1], **Catalina Simion**[1], **Pui-Yan Ho**[1], **Neelu Batra**[1], **Anastasia L. Berg**[1], **Kermit L. Carraway III**[1], **Aiming Yu**[1], **Colleen Sweeney**[1]

[1]Department of Biochemistry and Molecular Medicine, University of California, Davis, Sacramento, California, USA.

Abstract

miR-127 is downregulated in breast cancer, where it has been shown to suppress the proliferation, migration and invasion of breast cancer cells. In triple-negative breast cancer (TNBC), miR-127 downregulation correlates with decreased disease-free and overall patient survival. Tumor suppressor microRNAs may hold therapeutic promise but progress has been limited by several factors, including the lability and high cost of microRNA mimics. Here, we take a novel approach to produce a miR-127 pro-drug (miR-127PD), which we demonstrate is processed to mature, functional microRNA-127-3p in TNBC tumor cells. miR-127PD decreased the viability and motility of TNBC cells, sensitized TNBC cells to chemotherapy, and restricted the TNBC stem cell population. Furthermore, systemic delivery of miR-127PD suppressed tumor growth of MDA-MB-231 and MDA-MB-468 TNBC cells and spontaneous metastasis of MDA-MB-231 cells. In addition, CERK, NANOS1, FOXO6, SOX11, SOX12, FASN, and SUSD2 were identified as novel, functionally important targets of miR-127. In conclusion, our study demonstrates that miR-127 functions as a tumor and metastasis suppressor in triple-negative breast cancer and that delivery of miR-127 may hold promise as a novel therapy.

Keywords

miR-127; pro-drug; triple negative; metastasis

INTRODUCTION

MicroRNAs are small (~18–22 nt) non-coding RNAs which regulate gene expression through mRNA binding, most commonly within the 3'UTR, leading to mRNA destabilization and degradation (1). Each microRNA (miR) is capable of regulating hundreds of mRNAs and > 60% of human mRNAs have conserved at least one miR binding site (2). The ability of miRs to efficiently regulate gene *networks* makes them attractive for their therapeutic potential (3).

Corresponding author: Dr. Colleen Sweeney, Department of Biochemistry and Molecular Medicine, UC Davis Medical Center, Research Building III, 4645 2nd Avenue, Sacramento, California, USA, 95817, casweeney@ucdavis.edu.

The authors declare no potential conflict of interest.

In cancer, it is appreciated that miRs may function as either oncogenes (oncomiRs) or tumor suppressors (2). miR-127 was the first microRNA found to be epigenetically regulated, with its expression silenced in human cancer cell lines and primary tumors (4). Most studies have found that miR-127 has tumor suppressor properties, including studies performed in gastric (5), pancreatic (6), ovarian (7) and esophageal cancers (8) as well as hepatocellular carcinoma (9) and osteosarcoma (10). However, some studies including those in glioblastoma (11) and lung cancer (12), support an oncogenic function for miR-127.

In breast cancer, miR-127 is downregulated in primary tumors, compared to normal tissue, and expression of miR-127 mimics were shown to decrease the proliferation, migration and invasion of breast cancer cells through suppression of BCL6 (13,14). Recently, the miR-127 promoter was demonstrated to be hypermethylated in breast cancer, with increased frequency in poorly differentiated tumors of advanced stage (15). A significant correlation was observed between miR-127 hypermethylation in primary tumors and the presence of lymph node and/or distal metastases (15). Together, these findings suggest that silencing of miR-127 may promote metastasis. Therefore, restoration of miR-127 in breast cancer may hold therapeutic promise.

In this study, we utilize methods developed by Wang et al. (16) to bioengineer a novel miR-127 “pro-drug” that we demonstrate is processed to mature, functional miR-127-3p in breast cancer cells. The miR-127 pro-drug (miR-127^{PD}) has several advantages over synthetic/commercial microRNA mimics, including ease of expression, low cost, renewability as a resource, and lack of artificial chemical modifications. We focus on triple-negative breast cancer (TNBC), an aggressive subtype of breast cancer that relies mainly on cytotoxic chemotherapy for management. A major emphasis of research in TNBC since its recognition and definition as a breast cancer subtype has been the identification of targeted approaches and/or approaches which may sensitize cancer cells to chemotherapy, decreasing the burden of toxicity for patients (17). We demonstrate that miR-127^{PD} reduces the viability and stemness of TNBC cells *in vitro* and sensitizes TNBC cells to chemotherapy. Furthermore, delivery of miR-127^{PD} *in vivo* decreases tumor growth and inhibits lymph node and lung metastasis. Finally, we provide unique insight into the tumor suppressor function of miR-127, revealing new targets.

MATERIALS AND METHODS

Cell culture

MDA-MB-231 (Cat# HTB-26, RRID: CVCL_0062), MDA-MB-157 (Cat# HTB-24, RRID: CVCL_0618), MDA-MB-468 (Cat# HTB-132, RRID: CVCL_0419), HCC1937 (Cat# CRL-2336, RRID: CVCL_0290), nMuMG (Cat# CRL-1636, RRID: CVCL_0075), MCF-7 (Cat# HTB-22, RRID: CVCL_0031), and ZR-75-1 (Cat# CRL-1500, RRID: CVCL_0588) cells were purchased from American Type Culture Collection (ATCC) and maintained as recommended. HMEC4 and HMEC6 were gifted by K. Rao and maintained as described (18). Cell lines were authenticated by short tandem repeat profiling through the University of Arizona Genetics Core within the last 3 months. Cell lines were not tested for mycoplasma. Cells were used for 6–8 passages, after which they were replaced with a cryopreserved stock.

Expression and purification of miR-127^{PD}

Control (CTRL) and miR-127^{PD} constructs (Supplemental Figure S1) were produced using non-coding RNA bioengineering technology, as previously described (19). The sequence of miR-127 was obtained from miRBase (www.mirbase.org). The DNA fragment encoding miR-127 and its complementary passenger sequence (Supplemental Table S1) was cloned into pBSTNAV (provided by Dr. Luc Ponchon, Universite Paris Descartes, (20)) using SacII and EagI restriction sites (New England Biolabs, Cat# R0157, R0505). Plasmids were sequence verified (Genscript) and amplified in the DH5α strain. Recombinant ncRNA was expressed in HST08 E. coli and analyzed by denaturing urea (8 M) polyacrylamide (8%) gel electrophoresis (PAGE). Total bacterial RNA was isolated by phenol extraction. Anion exchange FPLC purification of miR-127^{PD} was performed on an NGC QUEST 10PLUS FPLC system (BioRad, Cat# 7880003) consisting of a fraction collector using a combination of Enrich-Q 10×100 and Bio-Scale Mini Macro-Prep DEAE columns (20). Purified recombinant ncRNAs were precipitated with ethanol then resuspended in nuclease-free water. Amicon ultra-0.5 mL centrifugal filters (30 KD; EMD Millipore, Cat# Z677892) were used for desalting and concentrating the RNA. RNA concentrations were measured using a NanoDrop 2000 Spectrophotometer (Thermo Fisher Scientific), and RNA purity was further determined by high performance liquid chromatography (HPLC) (16).

RNA isolation and quantitative real-time RT–PCR

Total RNA including miRNAs was collected using the miRNeasy Mini Kit (Qiagen, Cat# 217004) or TRIzol reagent (Invitrogen, Thermo Fischer Scientific, Cat# 15596026) according to the manufacturers' protocols. Tissues were homogenized in TRIzol reagent by Dounce homogenizer. For miR-127-3p expression qPCR, RNA was extracted from cells (MDA-MB-231, MDA-MB-157, MDA-MB-468, and HCC1937) that had been reverse-transfected with 10 nM of CTRL or miR-127^{PD} and from mice tissues (tumor, lung, and liver) which received systemic treatment of CTRL or miR-127^{PD}. TaqMan microRNA Reverse Transcription Kit (Applied Biosystems, Thermo Fischer Scientific, Cat# 4366596) was used to convert 10 ng RNA into cDNA. For validation of targets identified by RNA sequencing, RNA was extracted from MDA-MB-468 cells which had been reverse-transfected with 10 nM of CTRL or miR-127^{PD}, as well as tumor tissue from mice which received systemic treatment of CTRL or miR-127^{PD}. High-Capacity cDNA Reverse Transcription Kit (Applied Biosystems, Thermo Fischer Scientific, Cat# 4368814) was used to convert 1 μg of total RNA to cDNA. Quantitative PCR amplifications were conducted in a CFX96 real-time PCR system (BioRad) using reverse transcription primers and probes for miR-127-3p (Applied Biosystems, Thermo Fischer Scientific, Cat# 00452), gene-specific SYBR primers for CERK, NANOS1, SOX11, SOX12, FOXO6, FASN, SUSD2, ROCK2, and glyceraldehyde-3-phosphate dehydrogenase (GAPDH) (Supplemental Table S1), and iTaq Universal SYBR Green Supermix (BioRad, Cat# 1725120). Message levels for miR-127-3p were normalized to the U6 small nuclear RNA (RNU6B) (Applied Biosystems, Thermo Fischer Scientific, Cat# 001093). Message levels for CERK, NANOS1, SOX11, SOX12, FOXO6, FASN, SUSD2, and ROCK2 were normalized to (GAPDH). Analysis was performed by the comparative Ct method under the following cycling conditions: 30 seconds at 95°C, 40 cycles of 5 seconds at 95°C and 30sec at 60°C. Relative abundance was

determined from the Ct values using the $2^{-\Delta\Delta Ct}$ method after normalization to U6 or GAPDH.

Cell viability assay, cell proliferation assay, and chemotherapeutic cytotoxicity assay

Viability was evaluated using the 3-(4,5-Dimethyl-2-thiazolyl)-2,5-diphenyl-2H-tetrazolium bromide (MTT) (Sigma-Aldrich, Cat# M5655) assay per the manufactures' instructions. Cells were seeded in 96-well plates at 7.5–10×10^3 cells per well and reverse-transfected with CTRL or miR-127^{PD} for 72 hours, followed by the MTT assay. For assessment of proliferation, cells were seeded in 96-well plates at 2.5–5×10^3 cells per well and reverse-transfected with CTRL or miR-127^{PD}. MTT assay was conducted at 24-hour time intervals over the course of 5 days. For drug cytotoxicity assay, cells were seeded in 96-well plates at 7.5–10×10^3 cells per well and reverse-transfected with CTRL or miR-127^{PD}. After 24 hours, culture media was replaced with media containing Docetaxel (Selleckchem, Cat# S1148), Doxorubicin (Adriamycin) HCL (Selleckchem, Cat# S1208), Cisplatin (Sigma-Aldrich, Cat# 479306), or 5-Fluorouracil (Alfa Aesar, Thermo Fisher Scientific, Cat# A13456). Cells were incubated with chemotherapeutics for an additional 48 hours, followed by a MTT assay. The IC values were estimated by fitting the data to a four-parameter dose-response model ('drc' package, R). For rescue experiments, cells were seeded in 96-well plates at 1×10^4 cells per well for 16–18 hours prior to co-transfection with CTRL or miR-127^{PD} and 250 ng of Empty control vector (EV) (Cat# EX-NEG-MG13), CERK (Cat# EX-T3553-M13), NANOS1 (EX-Y2459-M13), SOX11 (EX-M0425-M13), or SOX12 (EX-Z5717-M13) plasmid DNA vectors (GeneCopoeia) for 72 hours, followed by the MTT assay. For all assays cells were reverse-transfected with 10nM CTRL or 10nM miR-127^{PD} using Lipofectamine 3000 (Invitrogen, Thermo Fischer Scientific, Cat# L3000008).

Antibodies and Western Blot analysis

For assessment of BCL6 protein abundance, cells were seeded in 12-well plates at 2.5×10^5 cells per well and reverse-transfected with 10nM CTRL or 10nM miR-127^{PD} using Lipofectamine 3000 for 72 hours. Total protein was extracted from cells using RIPA lysis buffer (50mM Tris (pH 7.4), 150mM NaCl, 0.1% SDS, 1% TritonX-100, 0.5% NaDeoxycholate). After incubation on ice, cells were scraped from wells, lysates were vortexed and centrifuged at 13,000 x g for 15 min. Lysate supernatants were placed into new microcentrifuge tubes and protein concentrations were determined using BCA kit (Pierce, Rockford, IL, USA). A unit of 15μg of cell lysate was denatured in 6X Laemmli sample buffer ((50 mmol l^{-1} Tris-HCl (pH 6.8), 2% SDS, 10% glycerol, 0.25% β-mercaptoethanol and bromophenol blue (1 $mgml^{-1}$)) at 100°C for 5 minutes. 2X Laemmli sample buffer was added to samples to bring to a final volume of 40μL. Samples were separated on an 8% SDS-polyacrylamide gel, and then transferred to nitrocellulose membrane (Millipore, Billerica, MA, USA). Membranes were blocked with 5% non-fat dry milk in TBST (Tris-buffered saline containing 0.05% Tween 20), and incubated with either anti-BCL6 (D4I2V) XP (Cell Signaling Technologies, Cat# 14895) or anti-β-Actin (AC-15) (Sigma-Aldrich, Cat# A1978) primary antibodies overnight at 4°C. After incubation, membranes were washed with TBST, and then incubated with horseradish peroxidase-conjugated secondary antibodies for one hour at room temperature. Chemiluminescence signal were visualized using ECL (Pierce) on an Alpha Innoteceh Digital Imaging Station. Blot images are a

representation of two technical replicates from samples acquired from two biological replicates.

Boyden Chamber Cell Migration Assay

MDA-MB-231 cells were seeded in 12-well plates at 2.5×10^5 cells per well and reverse-transfected with 10nM CTRL or 10nM miR-127^{PD} using Lipofectamine 3000. 16–24 hours later cells were detached and seeded into the upper chamber of the transwell insert (8μm-pore polycarbonate membranes (Corning, Cat# 3422)) at a density of 1×10^5 cells in serum-free DMEM, migrating toward the lower chamber containing DMEM with 10% FBS. After 24 hours migrated cells were fixed and stained using 100% methanol and 0.5% Crystal Violet, respectively. Migrated cells were imaged (three microscopic fields per membrane) using an Olympus IX81 inverted microscope and cellSens software (Olympus, RRID: SCR_016238). After imaging, membranes were removed and incubated in 10% acetic acid to solubilize Crystal Violet stain. Absorbance of Crystal Violet was measured using a microplate reader.

Tumorsphere Formation Assay

MDA-MB-231, MDA-MB-157, MDA-MB-468, and HCC1937 cells were seeded in 12-well plates at 2.5×10^5 cells per well and reverse-transfected with 10nM CTRL, miR-34a^{PD}, or miR-127^{PD} using Lipofectamine 3000. 16–24 hours later cells were plated in Corning Costar ultra-low attachment (ULA) 24-well plates (Sigma-Aldrich, Cat# CLS3473) with serum-free MammoCult media (Stem Cell Technologies, Cat# 05620) at a density of 2.5–5×10^3 cells per well and allowed to grow for 7 days. Following this, primary spheres (larger than 75 μm) were quantified and subsequently dissociated into a single cell suspension by trypsinization. Cells from dissociated primary spheres were re-plated in ULA plates and allowed to grow for another 7 days. Following this incubation, secondary spheres (larger than 75 μm) were quantified. Images were captured using an Olympus IX81 inverted microscope and cellSens software (Olympus, RRID: SCR_016238).

Animal Study

Animal studies were performed according to the protocols approved by the Institutional Animal Care and Use Committee of the University of California, Davis (Sacramento, CA). Six-week-old female non-obese diabetic/severe combined immunodeficient (NOD/SCID) mice (NOD.CB17-Prkdcscid/J, Cat# 001303, RRID: IMSR_JAX:001303) were purchased from The Jackson Laboratory, and were allowed to acclimate for one week before use. Orthotopic xenografts were established by bilateral subcutaneous injection into the fourth mammary fat pad of mice with MDA-MB-231 or MDA-MB-468 cell suspensions (2.8×10^6 cells or 5×10^6 cells, respectively) in a 1:1 volume/volume mixture of 10% sucrose/PBS solution and Matrigel GFR (Corning, Cat# 354230). Body weights were recorded twice weekly. Mammary tumors were measured twice weekly using digital calipers, and tumor volume was calculated according to the following formula: (Width^2 x Length) x 0.5. When tumor volume reached an average of 200 mm^3 (MDA-MB-231) and 70mm^3 (MDA-MB-468), mice were randomized into two treatment groups based on tumor volume (n = 10 mice per group): CTRL, miR-127^{PD}. Mice were dosed intravenously via lateral tail vein injection with a 40 μg loading dose followed by 30 μg maintenance doses (three times per

week for three weeks) of CTRL or miR-127^{PD} formulated with in vivo-jetPEI (Polyplus Transfection, Cat# 201-10G). At the study endpoint, mice were humanely euthanized according to our approved protocol and blood was collected via cardiac puncture and processed to serum for quantification of Alanine Transaminase (ALT), Aspartate Transaminase (AST), Blood Urea Nitrogen (BUN), Creatinine, and Total Bilirubin (Comparative Pathology Laboratory, UC Davis). Mammary tumors, lymph node, lung, and liver tissue were collected and either snap-frozen for RNA isolation or fixed in 10% neutral buffered formalin for paraffin embedding.

Histology and Immunohistochemistry

Histological analysis of primary tumors was performed for a randomly selected subset of CTRL and miR-127^{PD} tumors. Immunohistochemistry was performed as described (21). Anti-Ki-67 (1:500) (Cell Signaling Technologies, Cat# 9027), anti-cleaved Caspase 3 [Asp175] (1:500) (Cell Signaling Technologies, Cat# 9661), anti-human mitochondria [113-1] (1:1000) (Abcam, Cat# ab92824), anti-CyclinD1 (Novus Biologicals, Cat# NB100-79920) (1:100), anti-Vimentin (Gentex, Cat# GTX100619) (1:300), anti-Twist1/2 (Genetex, Cat# GTX127310) (1:200), and anti-N-Cadherin (Epitomics, Cat# 2447-1) (1:100), primary antibodies were used. An internal negative control (no primary antibody) was included with each trial. Images of 4 – 6 randomized fields of view per animal were captured then quantified using H DAB color deconvolution software in Image J Fiji (National Institutes of Health, RRID: SCR_002285). For analysis of tumor cell infiltration into lymph node tissue (n = 14), Image J software was used to quantify the total area of the lymph node compared to the total area comprised of tumor cells.

In silico analysis of human breast cancer data

Computational analysis was performed on publicly accessible data generated by The Cancer Genome Atlas (TCGA) Research Network (RRID: SCR_003193) or NCBI Gene Expression Omnibus (RRID: SCR_005012). Sequencing read counts or log2-transformed expression signal were used to determine levels of miR-127 expression, in adjacent normal versus breast tumor samples, across breast tumor molecular subtypes, and in primary breast tumors versus lymph node metastases. Welch two-sample t-test, and ANOVA followed by a Tukey HSD test, was used to determine whether the means of the two groups, or three or more groups, respectively, were statistically different. Kaplan–Meier survival plots were generated using the ‘survival’ and ‘survminer’ packages in the R statistical program. Data for Kaplan–Meier plots consisted of miR-127 expression (GSE59829) or miR-127 read count (TCGA) and patient information (GSE59829: death status and months of disease-free survival, TCGA: death status and days to last contact). Patients were ranked based on the descending level of miR-127 expression. Using data driven cut-offs computed by survminer, the top two-fifths (GSE59829) and two-thirds (TCGA) of patients were placed into the ‘High miR-127’ group. Tarone–Ware test (G-rho family of Harrington and Fleming survival test) was used to determine whether the difference in survival probability between groups was statistically different.

RNA sequencing and sequencing analysis

MDA-MB-468 cells were reverse-transfected in triplicate with 10 nM of CTRL or miR-127^{PD}. Total RNA was isolated using TRIzol-chloroform extraction according to the manufacturer's protocol at 36 hours post-transfection and RNA integrity was assessed by 1% agarose gel electrophoresis. Small RNAs: Library construction was prepared by BGI (Beijing Genomics Institute) starting with 1 μg of total RNA. Small RNA isolation was achieved by gel separation and purification, followed by the ligation of adenylated 3' adapters with unique barcodes to the RNA fragments. The product was expanded by PCR amplification, followed by a second size selection to avoid nonspecific products, selecting for 103–115 bp fragments by gel separation. Product yield was quantified by Qubit (Invitrogen, Thermo Fisher Scientific, Cat# Q33216) and samples were pooled to make a single strand DNA circle (ssDNA circle) to yield the final small RNA library. Rolling circle replication (RCR) was used to enlarge fluorescent signals for sequencing and single-end reads of 50 bp were read on the BGISEQ-500 platform. FASTQ-files were analyzed using the miRDeep module (22) to obtain the read counts of known miRNAs. An in-house PERL script was developed to map isoform fragment sequences corresponding to miR-127-3p. Differentially expressed miRNAs were discovered using the EdgeR package (23). miRNAs were considered to be significantly different between groups if P-value was < 0.05, Counts Per Million (Log10CPM) > 5, and the absolute Log2 of Fold Change (Log2FC) was greater than 20%. Messenger RNAs: mRNAs were purified using poly-T oligo-attached magnetic beads and fragmented by divalent cations, for first strand cDNA synthesis by use of random primers for reverse transcription, followed by second strand cDNA synthesis using DNA Polymerase I and RNase H. After subsequent ligation of 3' adapters to fragment ends, the products were then purified and enriched with PCR amplification and similarly quantified with Qubit. Stepwise sequencing was performed using the combinatorial Probe-Anchor (cPAL) ligation approach and read on the BGISEQ-500 system. FASTQ-files were analyzed using a combination workflow of BWA-RSEM-EdgeR (23). Sequence reads were mapped to the reference human-genome assembly (Feb. 2009, GRCh37/hg19) with BWA software. Sequence read counts for individual genes were computed using RSEM, and the resulting read counts from individual samples were subjected to the detection of differentially expressed mRNAs between phenotypes using EdgeR. mRNAs were considered to be significantly different if P-value < 0.05, Log10CPM > 5, and Log2FC > 20% greater. Networks, functions, and pathways analyses were generated using Ingenuity Pathway Analysis (Ingenuity Systems; Qiagen, Cat# 830025), primarily based on experimentally demonstrated interactions in human and rodent studies. Gene Set Enrichment Analysis (GSEA) was generated using GSEA v4.0.1 (Broad Institute, Inc., Massachusetts Institute of Technology). Differentially expressed transcripts were analyzed for the presence of Hallmark gene set enrichments. Normalized Enrichment Score (NES) and nominal (NOM) p-value were reported.

Statistical Analysis

Statistical tests for data analysis included Welch two-sample t-test, ANOVA followed by Tukey HSD test, log-rank test, and Student's t-test. Values are represented as mean ± standard error of the mean (SEM). For *in vitro* experiments, data represent at least three biological replicates containing at minimum duplicate technical replicates (unless otherwise

specified in the figure legend). For *in vivo* experiments, data represent 4–10 mice per experimental group. For IHC analysis, data represent 3–8 mice per experimental group (primary tumor analysis), and 7–8 mice per experimental group (lung/lymph node analysis). In all cases, differences were considered statistically significant when p-value was less than 0.05. All graphical representation and statistical analyses of data were performed using the R statistical program or Microsoft Excel. Images panels were assembled in Microsoft PowerPoint with brightness and contrast modifications made only for image clarity.

RESULTS

miR-127 expression in breast cancer

Prior studies indicated that miR-127 is downregulated in breast cancer (13,14). To see if this expression pattern holds in a larger sample set, we took advantage of the TCGA BRCA dataset. Available normal (n = 103) and breast tumor samples (n = 1101) were analyzed. As shown in Figure 1A, analysis of miRNA-seq data in the BRCA dataset revealed reduced expression of miR-127 in breast tumors relative to normal tissue. When tumors are classified into molecular subtypes (based on PAM50 subtyping (24)) basal tumors, of which ~ 90% are triple-negative (25), demonstrate low expression of miR-127 (Figure 1B). This was confirmed through analysis of an independent dataset, in which miR-127-3p expression was also found to be low in basal tumors (Supplementary Figure S2A, data from GSE19536 (26)). In addition, expression of miR-127-3p is further decreased in lymph node metastases relative to primary tumors of patients with triple-negative breast cancer (Figure 1C, data from GSE38167), suggesting that loss of miR-127 may be important in the TNBC metastatic process. Kaplan-Meier analysis of breast cancer patients was performed next to assess whether there was a correlation between miR-127 expression and disease-free survival (DFS) (data from GSE59829, (27)). Notably, patients whose breast tumors expressed higher levels of miR-127 had significantly increased DFS time compared to patients with lower miR-127 (Figure 1D), strongly suggesting that miR-127 expression is functionally important. This association was also observed through analysis of samples in the TCGA BRCA dataset, in which high miR-127 expression was significantly correlated with increased overall survival (Supplementary Figure S2B). Collectively, these results support the role of miR-127 as a tumor suppressor miRNA in breast cancer.

Production and purification of miR-127^{PD}

Given the need for new therapeutic approaches in TNBC, we decided to explore the potential of miR-127 in TNBC preclinical models. We first created a method for delivering miR-127 *in vitro* and *in vivo*. We took advantage of a recombinant RNA system developed and well-characterized by the Yu lab (16,28,29). This system uses an optimized tRNA scaffold and leads to the robust expression of the mature microRNA of choice. The details of construct generation are depicted in Supplementary Figure S1A and described in the methods section. The control construct, referred to as CTRL, contains an unconjugated tRNA scaffold. miR-127^{PD} was expressed in bacteria and purified by FPLC (Supplemental Figure S1B). Purity of isolated CTRL and miR-127^{PD} was confirmed by HPLC analysis (Supplemental Figure S1C). To determine whether miR-127^{PD} leads to the expression of mature miR-127, four different TNBC cell lines were transfected with CTRL or miR-127^{PD}

constructs. Transfection of miR-127^{PD} led to robust expression of miR-127-3p, in all four TNBC cell lines, as determined by stem-loop qPCR (Figure 2A). According to deep sequencing results collated from 134 experiments at miRbase, 3p is the dominant arm for miR-127 by a factor of ~ 558-fold over the 5p arm.

miR-127^{PD} decreases viability of TNBC cells

We next examined the impact of miR-127^{PD} expression on the viability of TNBC cells. HCC1937 cells, which are homozygous for the BRCA1^{5382C} mutation, were included to represent BRCA-mutant TNBC. miR-127^{PD} significantly decreased the viability of all four TNBC cell lines (Figure 2B and C) while no discernable effects of the CTRL on TNBC cell viability were observed (Supplemental Figure S3A). miR-127^{PD} had only modest impact on the viability of normal human and mouse mammary epithelial cell lines (Supplemental Figure S3B). miR-127^{PD} also significantly decreased the viability of two luminal (non-TNBC) cell lines (MCF-7 and ZR75-1) (Supplemental Figure S3C). As expected, miR-127^{PD} decreased the abundance of the cell survival protein BCL6, in all four TNBC cell lines (Supplemental Figure S3D and E). BCL6 was the first validated target of miR-127-3p but notably, is regulated by translational repression rather than mRNA destabilization (4). Our data is in agreement with this as we found down-regulation of BCL6 protein but not mRNA (Supplemental Figure S3F).

We next examined the impact of miR-127^{PD} on the cancer stem cell (CSC) subpopulation, which has been implicated in metastasis, disease relapse and therapeutic resistance (30). We utilized the tumorsphere assay, a well-accepted and widely used functional assay for stem cells (31). As shown in Figure 2D and E, sphere-forming ability of cells from the four TNBC cell lines was remarkably decreased by miR-127^{PD}. We also compared miR-127^{PD} to miR-34a^{PD} (28,29), as miR-34a is a well-established tumor suppressor (32) also downregulated in TNBC (33), and found miR-127^{PD} to be more effective at reducing sphere forming capacity.

miR-127^{PD} sensitizes TNBC cells to cytotoxic chemotherapy

Cytotoxic chemotherapy is the mainstay of TNBC management, however, the majority of TNBC patients are resistant to chemotherapy. For these non-responsive patients there is a significantly elevated risk of death compared to the small subset of TNBC patients who do respond to chemotherapy (34). Therefore, we next examined whether miR-127^{PD} expression was capable of sensitizing TNBC cells to chemotherapy agents commonly used for TNBC management, according to NCCN.org (the National Comprehensive Cancer Center Network). Cells treated with miR-127^{PD} were consistently more sensitive to Docetaxel, Doxorubicin, Cisplatin, and 5-Fluorouracil (Figure 3A and B). Moreover, miR-127^{PD} treatment reduced the IC_{50} for each chemotherapeutic (Supplemental Table S2). Because cancer stem cells are thought to underlie disease relapse, their eradication is a high priority in oncology (30). As such, we examined the impact of miR-127^{PD} on the chemosensitivity of the CSC subpopulation, using the tumorsphere assay. Expression of miR-127^{PD} significantly sensitized TNBC CSCs to three different chemotherapeutic agents (Figure 3C and D).

miR-127^{PD} suppresses primary tumor growth and spontaneous metastasis *in vivo*

We next examined the impact of miR-127^{PD} delivery on the growth of both MDA-MB-231 and MDA-MB-468 cells *in vivo* using an orthotopic (mammary fat pad) xenograft model. CTRL and miR-127^{PD} were delivered via tail vein injection using methods optimized by the Yu lab (16,28,29). The experimental timeline is depicted in Figure 4A. The cohorts of mice which received miR-127^{PD} demonstrated a statistically significant decrease in tumor growth compared to the cohort that received CTRL (Figure 4B and C). qRT-PCR analysis indicated that mature miR-127-3p accumulated in primary tumors of mice treated systemically with miR-127^{PD} (Figure 4D). Since the lungs and liver are preferred sites of metastasis in TNBC (35), we also analyzed the level of miR-127-3p in these organs. We found that mature miR-127-3p significantly accumulated in the lungs and livers of miR-127^{PD}-treated mice as compared to CTRL-treated mice (Figure 4D). Primary tumors from mice treated with miR-127 showed less evidence of proliferation, as assessed by Ki67 immunohistochemistry, and for MDA-MB-231 cells, more evidence of apoptosis as assessed by cleaved-caspase-3 staining (Figure 4E and F). Further, expression of Cyclin D1, a driver of the G1/S cell cycle transition and a breast cancer oncogene was decreased in MDA-MB-231 primary tumors from mice treated with miR-127^{PD} (Supplemental Figure S4A). Importantly, there was no significant change in body weight between CTRL and miR-127^{PD} groups over the course of treatment (Supplemental Figure S4B). Additionally, treatment did not deleteriously impact kidney or liver function, with blood chemistry values remaining in the normal range (Supplemental Table S3).

TNBC patients have a significantly higher risk of distant relapse compared to other breast cancer subtypes (35,36). Our *in silico* analysis indicated that miR-127-3p is significantly downregulated in lymph node metastases relative to TNBC primary tumors (Figure 1C), suggesting that miR-127 loss may contribute to metastasis. As cell motility is essential to metastasis, we first examined the effects of miR-127^{PD} on MDA-MB-231 cell migration in a Boyden chamber assay. miR-127^{PD} significantly decreased the migration of these cells compared to CTRL (Supplemental Figure S4C). We next examined the effect of miR-127^{PD} delivery on spontaneous metastasis. Metastatic (human) MDA-MB-231 cells were detected in lymph nodes and lungs using a human-specific anti-mitochondrial antibody (Figure 5A and B). We observed that mice treated systemically with miR-127^{PD} showed decreased lung metastasis (Figure 5A and C–D). Additionally, axillary lymph node tissue showed significantly less infiltration by MDA-MB-231 cells (Figure 5B and E). We did not observe metastases for MDA-MB-468 cells during the time period of our study, in agreement with many prior reports that the parental cells are poorly metastatic (37).

Identification of the miR-127-regulated miRNome and transcriptome

To gain insight into the functional impact of miR-127 on TNBC cells, we performed small RNA sequencing analysis of MDA-MB-468 cells treated with CTRL or miR-127^{PD}. Our analysis demonstrated that miR-127^{PD} was processed to mature miR-127-3p and accumulates substantially in cells (Figure 6A, top closed circle). Expression of miR-127^{PD} led to a specific change in the miRNome profile, in which miR-127-3p became the second most abundant miRNA (Figure 6B). While Figure 6B highlights the comprehensive alterations in the miRNome as a whole, it is worth noting that mature miR-127-3p

expression was increased 1347-fold following miR-127^{PD} treatment (Supplemental Figure S5). We also observed 17 miRNAs to be significantly upregulated and 11 downregulated after miR-127^{PD} treatment (Figure 6A, Supplemental RNASeq File 1). Notably, 66.7% of the upregulated small RNAs and 71.4% of downregulated small RNAs, have been previously identified as tumor suppressor miRs or oncomiRs, respectively.

To examine changes to the transcriptome resulting from miR-127 expression, we also performed mRNA sequencing on the same samples described above. Sequencing analysis showed that 284 transcripts were significantly downregulated and 425 upregulated following miR-127 expression (Figure 7A, Supplemental RNASeq File 2). The top ~10% of downregulated transcripts are highlighted in Figure 7B. We independently validated a subset of these, all of which are *novel* putative targets of miR-127, including ceramide kinase (CERK), NANOS1, SOX11, SOX12, FOXO6, fatty acid synthase (FASN), and sushi domain containing 2 (SUSD2)) by qPCR in MDA-MB-468 cells (Figure 7C). Notably, 75.7% of the significantly downregulated mRNAs are predicted to be direct targets of miR-127-3p, based on miRNA target prediction tools (microRNA.org, miRWALK, and miRMAP). Rho-associated protein kinase 2 (ROCK2), which was previously shown to be downregulated by miR-127-5p mimics (38), was not downregulated in our analysis (Figure 7A–C), serving as an internal control for 3p specificity. Importantly, with the exception of FASN in MDA-MB-231 tumors, these targets were downregulated in the primary tumors of both models treated systemically with miR-127^{PD} (Figure 7D). As our analyses are done at the end of the in vivo experiment and represent a “snapshot” in time, this could explain why we did not observe FASN downregulation in MDA-MB-231 tumors. To explore the functional interaction between miR-127 and these targets we chose four targets (CERK, NANOS1, SOX11 and SOX12) and performed “rescue” experiments. TNBC cells were co-transfected with CTRL or miR-127^{PD} and empty vector (EV) or vector containing CERK, NANOS1, SOX11, or SOX12 cDNAs. Because cDNAs lack a 3’UTR/miR-127 binding site, they are not regulated by miR-127 and reconstitute expression of the target. As expected, miR-127^{PD} significantly decreased the viability of all four TNBC cell lines compared to CTRL when co-transfected with EV plasmid (Figure 7E). While there were cell-dependent differences, NANOS1, SOX11 and SOX12 rescued viability in all four TNBC cell lines, with CERK rescuing in two of the four cell lines. Given that miR-127 regulates many targets, these experiments in which one target impacts miR-127 function underscores their likely importance.

Finally, we performed pathway analysis to gain further insight into miR-127 function. Pathways downregulated by miR-127 expression were linked to proliferation, cell cycle progression, cell adhesion and motility, migration and invasion, the epithelial-to-mesenchymal transition (EMT), chemoresistance, and stemness, while pathways upregulated by miR-127 expression were predominately linked to apoptosis (Supplemental Figure S6). GSEA (gene set enrichment analysis) also revealed epithelial to mesenchymal transition and apoptosis as hallmark (Supplemental Table 4). Interestingly, we observed that markers of EMT, including Vimentin, Twist and N-cadherin, were decreased in MDA-MB-231 tumors from animals treated with miR-127^{PD} (Supplemental Figure S7). Collectively, our data provide strong support for a tumor-suppressive role of miR-127 in TNBC, as well as novel insight into the molecular mechanisms that underlie miR-127 function.

DISCUSSION

Since the discovery of the first microRNA in *C. elegans* in 1993, the field has moved deliberately towards realizing the promise of microRNA as therapeutics. There is substantial evidence from preclinical studies that this promise will be realized, and several microRNAs are currently in Phase II clinical trials (39,40). To date, most studies have relied on chemically synthesized microRNA "mimics". However, these mimics have drawbacks, including the presence of artificial chemical modifications, intended to improve pharmacokinetics, yet often increasing immunogenicity and deleteriously impacting RNA folding and efficacy of target inhibition (41). In this study, we take advantage of a cost-efficient and renewable RNA bio-fermentation approach to produce our reagents. This strategy uses a tRNA-based scaffold first described by Ponchon *et al.* (20) and further optimized by the Yu lab (19), providing milligrams of reagent per liter of culture (41). Here, we demonstrate that miR-127^{PD} leads to the robust expression of *mature* miR-127-3p *in vitro* and *in vivo*.

While new therapies are emerging, cytotoxic chemotherapy will likely remain an essential aspect of TNBC management and is currently used in the neoadjuvant, adjuvant and metastatic settings (36). Compared to patients with other subtypes of breast cancer, TNBC patients are actually *more likely* to respond to chemotherapy (42); however, only one-third of TNBC patients achieve a pathological complete response (pCR) with the remaining two-thirds at *12-fold* elevated risk of death (34). This underscores the need for new approaches that sensitize TNBC cells to chemotherapy. Our studies are the first to demonstrate that miR-127-3p depletes the TNBC cancer stem cell (CSC) population, widely implicated in chemoresistance. Furthermore, we demonstrate that miR-127-3p sensitizes TNBC cells, including the CSC subpopulation, to TNBC-appropriate chemotherapeutic agents.

To determine whether miR-127^{PD} has activity *in vivo*, we orthotopically implanted MDA-MB-231 and MDA-MB-468 TNBC cells. We demonstrate that systemic delivery of miR-127^{PD} leads to the expression of miR-127-3p in primary tumors as well as lung and liver, common sites of metastasis for TNBC (35). To our knowledge, this is the first demonstration that intravenous delivery of a microRNA leads to its accumulation in tumors implanted in the mammary gland. Importantly, there was no evidence of toxicity throughout the study. While a prior publication reported that miR-127-5p mimics inhibit lung colonization of tail vein injected MDA-MB-231 cells, our studies are novel in that they demonstrate that miR-127-3p inhibits primary tumor growth in both our MDA-MB-231 and MDA-MB-468 TNBC models and *spontaneous* metastasis of MDA-MB-231 TNBC cells.

To gain insight into the molecular consequences of miR-127-3p expression, we performed RNAseq in MDA-MB-468 cells as they consistently exhibited the most robust response to miR-127^{PD} *in vitro*. RNAseq analysis revealed a shift in the miRnome of miR-127^{PD}-treated cells, with an increase in tumor suppressor microRNAs and a decrease in oncomiRs. We also identified novel mRNA targets of miR-127; seven of which we independently validated by qPCR and demonstrated to be down-regulated in tumors in miR-127^{PD} treated mice. Each of the seven is predicted to be a direct target of miR-127-3p and existing literature implicates them as important players in cancer.

CERK (ceramide kinase), which synthesizes ceramide-1-phosphate and promotes cell survival (43), is correlated with poor prognosis in ER-negative breast cancer (44) and is most highly expressed in the basal-like molecular subtype of breast cancer, which largely overlaps with TNBC (45). CERK was found to be upregulated in recurrent mammary tumors and to promote mammary tumor recurrence (44). NANOS1, a member of the highly evolutionary conserved Nanos family implicated in pluripotency, self-renewal and survival (46), is repressed by E-cadherin and promotes tumor cell invasion through regulation of MT1-MMP. Knockdown of NANOS1 in Bt549 TNBC cells was shown to decrease their invasion *in vitro* (47). SOX11, a member of the SOX family of transcription factors, is overexpressed in TNBC and is critical for growth, migration and invasion of TNBC cell lines, including the MDA-MB-231 and MDA-MB-468 cells used herein (48). In addition, SOX11 drives expression of genes which define basal-like breast cancer, and high SOX11 expression is associated with poor disease-specific, recurrence-free and metastasis-free survival in breast cancer (48). SOX11 has also been shown to increase the mammary stem cell and cancer stem cell populations of MCF10A and DCIS.com cells, respectively, and to increase invasive growth of DCIS.com cells *in vivo* (49). Less is known about SOX12 although it has been linked to cancer stemness in hepatocellular carcinoma (50). In breast cancer, SOX12 is overexpressed relative to normal tissue and knockdown was shown to inhibit *in vitro* migration/invasion and *in vivo* tumor growth of ER-positive breast cancer cells (51). FOXO6 is a member of the O-subfamily of FOXO transcription factors. Its role in breast cancer is not yet clear. One study found that FOXO6 is upregulated in breast cancer and high FOXO6 expression is correlated with poor metastasis-free survival in TNBC. This group also reported that knock-down of FOXO6 decreased proliferation of MDA-MB-468 and HCC38 TNBC cells (52). A second study reported conflicting results, with FOXO6 shown to be down-regulated in breast cancer and able to inhibit the migration/invasion of TNBC cells (53). Further studies are needed to resolve these findings. FASN (fatty acid synthase) has long been pursued as a therapeutic target in various cancers, including breast cancer; and clinical trials are ongoing (54). FASN is expressed in ~ 90% of TNBCs, with nearly half demonstrating overexpression, which correlates with lymph node positive status (55) and decreased distant metastasis-free survival (56). Of note, inhibition of FASN has been shown to sensitize MDA-MB-231 TNBC cells to 5-flurouracil (57), cisplatin (58) and docetaxel (59). SUSD2 (sushi domain containing 2), a transmembrane protein, is not detected in normal breast but is expressed in a majority of breast cancers, including TNBC (60). SUSD2 overexpression was shown to significantly increase the invasion of MDA-MB-231 TNBC cells *in vitro* and to increase tumor growth and metastasis of 66CL4 TNBC murine tumor cells *in vivo*. This study also found that SUSD2-overexpressing MDA-MB-231 cells promoted Jurkat T-cell apoptosis *in vitro*, suggesting a potential role in immune evasion. Collectively, our study contributes novel insight into the function of miR-127 in breast cancer and provides strong evidence that it holds promise as a novel therapy for TNBC.

Supplementary Material

Refer to Web version on PubMed Central for supplementary material.

ACKNOWLEGMENTS

We thank J.Q. Chen and Q. Zhang for technical assistance, and A.R. Rowson-Hodel for editorial assistance. We thank John D. McPherson for assistance with GSEA analysis. The authors also wish to thank the histology core facility at UC Davis for embedding mouse tissues, slide preparation, and performing the anti-human mitochondria immunohistochemistry analysis. We gratefully acknowledge the support of NIH/NCI R01CA225958 (A. Yu) and NIH/NIGMS R01GM113888 (A. Yu) and The National Academies of Sciences Engineering Medicine Ford Foundation Predoctoral Fellowship (M. Umeh-Garcia). The authors also appreciate the access to the Molecular Pharmacology Shared Resources funded by the UC Davis Comprehensive Cancer Center Support Grant (CCSG) awarded by the NIH/NCI (P30CA093373).

Financial support: NIH/NCI (R01CA225958), NIH/NIGMS (R01GM113888).

REFERENCES

1. Friedman RC, Farh KK-H, Burge CB, Bartel DP. Most mammalian mRNAs are conserved targets of microRNAs. Genome Res. 2009;19:92–105. [PubMed: 18955434]
2. Guo H, Ingolia NT, Weissman JS, Bartel DP. Mammalian microRNAs predominantly act to decrease target mRNA levels. Nature. 2010;466:835–40. [PubMed: 20703300]
3. Garzon R, Marcucci G, Croce CM. Targeting microRNAs in cancer: rationale, strategies and challenges. Nat Rev Drug Discov. 2010;9:775–89. [PubMed: 20885409]
4. Saito Y, Liang G, Egger G, Friedman JM, Chuang JC, Coetzee GA, et al. Specific activation of microRNA-127 with downregulation of the proto-oncogene BCL6 by chromatin-modifying drugs in human cancer cells. Cancer Cell. 2006;9:435–43. [PubMed: 16766263]
5. Guo L-H, Li H, Wang F, Yu J, He J-S. The Tumor Suppressor Roles of miR-433 and miR-127 in Gastric Cancer. Int J Mol Sci. 2013;14:14171–84. [PubMed: 23880861]
6. Yu Y, Liu L, Ma R, Gong H, Xu P, Wang C. MicroRNA-127 is aberrantly downregulated and acted as a functional tumor suppressor in human pancreatic cancer. Tumour Biol J Int Soc Oncodevelopmental Biol Med. 2016;37:14249–57.
7. Bi L, Yang Q, Yuan J, Miao Q, Duan L, Li F, et al. microRNA-127-3p acts as a tumor suppressor in epithelial ovarian cancer by regulating the BAG5 gene. Oncol Rep. 2016;36:2563–70. [PubMed: 27571744]
8. Gao X, Wang X, Cai K, Wang W, Ju Q, Yang X, et al. MicroRNA-127 is a tumor suppressor in human esophageal squamous cell carcinoma through the regulation of oncogene FMNL3. Eur J Pharmacol. 2016;791:603–10. [PubMed: 27645894]
9. Zhou J, Lu S, Yang S, Chen H, Shi H, Miao M, et al. MicroRNA-127 post-transcriptionally downregulates Sept7 and suppresses cell growth in hepatocellular carcinoma cells. Cell Physiol Biochem Int J Exp Cell Physiol Biochem Pharmacol. 2014;33:1537–46.
10. Zhang J, Hou W, Chai M, Zhao H, Jia J, Sun X, et al. microRNA-127-3p inhibits proliferation and invasion by targeting SETD8 in human osteosarcoma cells. Biochem Biophys Res Commun. 2016;469:1006–11. [PubMed: 26707641]
11. Jiang H, Hua D, Zhang J, Lan Q, Huang Q, Yoon J-G, et al. microRNA-127-3p promotes glioblastoma cell migration and invasion by targeting the tumor-suppressor gene SEPT7. Oncol Rep. 2014;31:2261–9. [PubMed: 24604520]
12. Shi L, Wang Y, Lu Z, Zhang H, Zhuang N, Wang B, et al. miR-127 promotes EMT and stem-like traits in lung cancer through a feed-forward regulatory loop. Oncogene. 2017;36:1631–43. [PubMed: 27869168]
13. Chen J, Wang M, Guo M, Xie Y, Cong Y-S. miR-127 regulates cell proliferation and senescence by targeting BCL6. PloS One. 2013;8:e80266. [PubMed: 24282530]
14. Wang S, Li H, Wang J, Wang D, Yao A, Li Q. Prognostic and biological significance of microRNA-127 expression in human breast cancer. Dis Markers. 2014;2014:401986. [PubMed: 25477702]
15. Pronina IV, Loginov VI, Burdennyy AM, Fridman MV, Senchenko VN, Kazubskaya TP, et al. DNA methylation contributes to deregulation of 12 cancer-associated microRNAs and breast cancer progression. Gene. 2017;604:1–8. [PubMed: 27998789]

16. Wang W-P, Ho PY, Chen Q-X, Addepalli B, Limbach PA, Li M-M, et al. Bioengineering Novel Chimeric microRNA-34a for Prodrug Cancer Therapy: High-Yield Expression and Purification, and Structural and Functional Characterization. J Pharmacol Exp Ther. 2015;354:131–41. [PubMed: 26022002]
17. Bianchini G, Balko JM, Mayer IA, Sanders ME, Gianni L. Triple-negative breast cancer: challenges and opportunities of a heterogeneous disease. Nat Rev Clin Oncol. 2016;13:674–90. [PubMed: 27184417]
18. Cheng J-M, Ding M, Aribi A, Shah P, Rao K. Loss of RAB25 expression in breast cancer. Int J Cancer. 2006;118:2957–64. [PubMed: 16395697]
19. Ho PY, Duan Z, Batra N, Jilek JL, Tu M-J, Qiu J-X, et al. Bioengineered Noncoding RNAs Selectively Change Cellular miRNome Profiles for Cancer Therapy. J Pharmacol Exp Ther. 2018;365:494–506. [PubMed: 29602831]
20. Ponchon L, Beauvais G, Nonin-Lecomte S, Dardel F. A generic protocol for the expression and purification of recombinant RNA in Escherichia coli using a tRNA scaffold. Nat Protoc. 2009;4:947–59. [PubMed: 19478810]
21. Rowson-Hodel AR, Wald JH, Hatakeyama J, O'Neal WK, Stonebraker JR, VanderVorst K, et al. Membrane Mucin Muc4 promotes blood cell association with tumor cells and mediates efficient metastasis in a mouse model of breast cancer. Oncogene. 2018;37:197–207. [PubMed: 28892049]
22. An J, Lai J, Lehman ML, Nelson CC. miRDeep*: an integrated application tool for miRNA identification from RNA sequencing data. Nucleic Acids Res. 2013;41:727–37. [PubMed: 23221645]
23. Robinson MD, McCarthy DJ, Smyth GK. edgeR: a Bioconductor package for differential expression analysis of digital gene expression data. Bioinforma Oxf Engl. 2010;26:139–40.
24. Parker JS, Mullins M, Cheang MCU, Leung S, Voduc D, Vickery T, et al. Supervised risk predictor of breast cancer based on intrinsic subtypes. J Clin Oncol Off J Am Soc Clin Oncol. 2009;27:1160–7.
25. Cheang MCU, Martin M, Nielsen TO, Prat A, Voduc D, Rodriguez-Lescure A, et al. Defining Breast Cancer Intrinsic Subtypes by Quantitative Receptor Expression. The Oncologist. 2015;20:474–82. [PubMed: 25908555]
26. Enerly E, Steinfeld I, Kleivi K, Leivonen S-K, Aure MR, Russnes HG, et al. miRNA-mRNA integrated analysis reveals roles for miRNAs in primary breast tumors. PloS One. 2011;6:e16915. [PubMed: 21364938]
27. D'Aiuto F, Callari M, Dugo M, Merlino G, Musella V, Miodini P, et al. miR-30e* is an independent subtype-specific prognostic marker in breast cancer. Br J Cancer. 2015;113:290–8. [PubMed: 26057454]
28. Zhao Y, Tu M-J, Yu Y-F, Wang W-P, Chen Q-X, Qiu J-X, et al. Combination therapy with bioengineered miR-34a prodrug and doxorubicin synergistically suppresses osteosarcoma growth. Biochem Pharmacol. 2015;98:602–13. [PubMed: 26518752]
29. Zhao Y, Tu M-J, Wang W-P, Qiu J-X, Yu A-X, Yu A-M. Genetically engineered pre-microRNA-34a prodrug suppresses orthotopic osteosarcoma xenograft tumor growth via the induction of apoptosis and cell cycle arrest. Sci Rep. 2016;6:26611. [PubMed: 27216562]
30. Shibue T, Weinberg RA. EMT, CSCs, and drug resistance: the mechanistic link and clinical implications. Nat Rev Clin Oncol. 2017;14:611–29. [PubMed: 28397828]
31. Lee C-H, Yu C-C, Wang B-Y, Chang W-W. Tumorsphere as an effective in vitro platform for screening anti-cancer stem cell drugs. Oncotarget. 2016;7:1215–26. [PubMed: 26527320]
32. Raver-Shapira N, Marciano E, Meiri E, Spector Y, Rosenfeld N, Moskovits N, et al. Transcriptional activation of miR-34a contributes to p53-mediated apoptosis. Mol Cell. 2007;26:731–43. [PubMed: 17540598]
33. Adams BD, Wali VB, Cheng CJ, Inukai S, Booth CJ, Agarwal S, et al. miR-34a Silences c-SRC to Attenuate Tumor Growth in Triple-Negative Breast Cancer. Cancer Res. 2016;76:927–39. [PubMed: 26676753]
34. Cortazar P, Zhang L, Untch M, Mehta K, Costantino JP, Wolmark N, et al. Pathological complete response and long-term clinical benefit in breast cancer: the CTNeoBC pooled analysis. Lancet Lond Engl. 2014;384:164–72.

35. Wu Q, Li J, Zhu S, Wu J, Chen C, Liu Q, et al. Breast cancer subtypes predict the preferential site of distant metastases: a SEER based study. Oncotarget. 2017;8:27990–6. [PubMed: 28427196]
36. Collignon J, Lousberg L, Schroeder H, Jerusalem G. Triple-negative breast cancer: treatment challenges and solutions. Breast Cancer Dove Med Press. 2016;8:93–107. [PubMed: 27284266]
37. Vantyghem SA, Allan AL, Postenka CO, Al-Katib W, Keeney M, Tuck AB, et al. A new model for lymphatic metastasis: development of a variant of the MDA-MB-468 human breast cancer cell line that aggressively metastasizes to lymph nodes. Clin Exp Metastasis. 2005;22:351–61. [PubMed: 16170671]
38. Uppal A, Wightman SC, Mallon S, Oshima G, Pitroda SP, Zhang Q, et al. 14q32-encoded microRNAs mediate an oligometastatic phenotype. Oncotarget. 2015;6:3540–52. [PubMed: 25686838]
39. Rupaimoole R, Slack FJ. MicroRNA therapeutics: towards a new era for the management of cancer and other diseases. Nat Rev Drug Discov. 2017;16:203–22. [PubMed: 28209991]
40. Yu A-M, Jian C, Yu AH, Tu M-J. RNA therapy: Are we using the right molecules? Pharmacol Ther. 2018.
41. Zhang H, Sun D-W, Mao L, Zhang J, Jiang L-H, Li J, et al. MiR-139–5p inhibits the biological function of breast cancer cells by targeting Notch1 and mediates chemosensitivity to docetaxel. Biochem Biophys Res Commun. 2015;465:702–13. [PubMed: 26299922]
42. Liedtke C, Mazouni C, Hess KR, André F, Tordai A, Mejia JA, et al. Response to neoadjuvant therapy and long-term survival in patients with triple-negative breast cancer. J Clin Oncol Off J Am Soc Clin Oncol. 2008;26:1275–81.
43. Gómez-Muñoz A, Kong JY, Parhar K, Wang SW, Gangoiti P, González M, et al. Ceramide-1-phosphate promotes cell survival through activation of the phosphatidylinositol 3-kinase/protein kinase B pathway. FEBS Lett. 2005;579:3744–50. [PubMed: 15978590]
44. Ruckhäberle E, Karn T, Rody A, Hanker L, Gätje R, Metzler D, et al. Gene expression of ceramide kinase, galactosyl ceramide synthase and ganglioside GD3 synthase is associated with prognosis in breast cancer. J Cancer Res Clin Oncol. 2009;135:1005–13. [PubMed: 19125296]
45. Payne AW, Pant DK, Pan T-C, Chodosh LA. Ceramide kinase promotes tumor cell survival and mammary tumor recurrence. Cancer Res. 2014;74:6352–63. [PubMed: 25164007]
46. De Keuckelaere E, Hulpiau P, Saeys Y, Berx G, van Roy F. Nanos genes and their role in development and beyond. Cell Mol Life Sci CMLS. 2018;75:1929–46. [PubMed: 29397397]
47. Bonnomet A, Polette M, Strumane K, Gilles C, Dalstein V, Kileztky C, et al. The E-cadherin-repressed hNanos1 gene induces tumor cell invasion by upregulating MT1-MMP expression. Oncogene. 2008;27:3692–9. [PubMed: 18223680]
48. Shepherd JH, Uray IP, Mazumdar A, Tsimelzon A, Savage M, Hilsenbeck SG, et al. The SOX11 transcription factor is a critical regulator of basal-like breast cancer growth, invasion, and basal-like gene expression. Oncotarget. 2016;7:13106–21. [PubMed: 26894864]
49. Oliemuller E, Kogata N, Bland P, Kriplani D, Daley F, Haider S, et al. SOX11 promotes invasive growth and ductal carcinoma in situ progression. J Pathol. 2017;243:193–207. [PubMed: 28707729]
50. Zou S, Wang C, Liu J, Wang Q, Zhang D, Zhu S, et al. Sox12 Is a Cancer Stem-Like Cell Marker in Hepatocellular Carcinoma. Mol Cells. 2017;40:847–54. [PubMed: 29127951]
51. Ding H, Quan H, Yan W, Han J. Silencing of SOX12 by shRNA suppresses migration, invasion and proliferation of breast cancer cells. Biosci Rep. 2016.
52. Lallemand F, Petitalot A, Vacher S, de Koning L, Taouis K, Lopez BS, et al. Involvement of the FOXO6 transcriptional factor in breast carcinogenesis. Oncotarget. 2018;9:7464–75. [PubMed: 29484124]
53. Ye H, Duan M. Downregulation of FOXO6 in breast cancer promotes epithelial-mesenchymal transition and facilitates migration and proliferation of cancer cells. Cancer Manag Res. 2018;10:5145–56. [PubMed: 30464613]
54. Menendez JA, Lupu R. Fatty acid synthase (FASN) as a therapeutic target in breast cancer. Expert Opin Ther Targets. 2017;21:1001–16. [PubMed: 28922023]

55. Giró-Perafita A, Sarrats A, Pérez-Bueno F, Oliveras G, Buxó M, Brunet J, et al. Fatty acid synthase expression and its association with clinico-histopathological features in triple-negative breast cancer. Oncotarget. 2017;8:74391–405. [PubMed: 29088795]

56. Corominas-Faja B, Vellon L, Cuyàs E, Buxó M, Martin-Castillo B, Serra D, et al. Clinical and therapeutic relevance of the metabolic oncogene fatty acid synthase in HER2+ breast cancer. Histol Histopathol. 2017;32:687–98. [PubMed: 27714708]

57. Vazquez-Martin A, Ropero S, Brunet J, Colomer R, Menendez JA. Inhibition of Fatty Acid Synthase (FASN) synergistically enhances the efficacy of 5-fluorouracil in breast carcinoma cells. Oncol Rep. 2007;18:973–80. [PubMed: 17786362]

58. Al-Bahlani S, Al-Lawati H, Al-Adawi M, Al-Abri N, Al-Dhahli B, Al-Adawi K. Fatty acid synthase regulates the chemosensitivity of breast cancer cells to cisplatin-induced apoptosis. Apoptosis Int J Program Cell Death. 2017;22:865–76.

59. Menendez JA, Lupu R, Colomer R. Inhibition of tumor-associated fatty acid synthase hyperactivity induces synergistic chemosensitization of HER −2/ neu -overexpressing human breast cancer cells to docetaxel (taxotere). Breast Cancer Res Treat. 2004;84:183–95. [PubMed: 14999148]

60. Watson AP, Evans RL, Egland KA. Multiple functions of sushi domain containing 2 (SUSD2) in breast tumorigenesis. Mol Cancer Res MCR. 2013;11:74–85. [PubMed: 23131994]

SIGNIFICANCE

Exogenous administration of miR-127 that is functionally activated in target cells inhibits growth and spontaneous metastasis of triple-negative breast cancer.

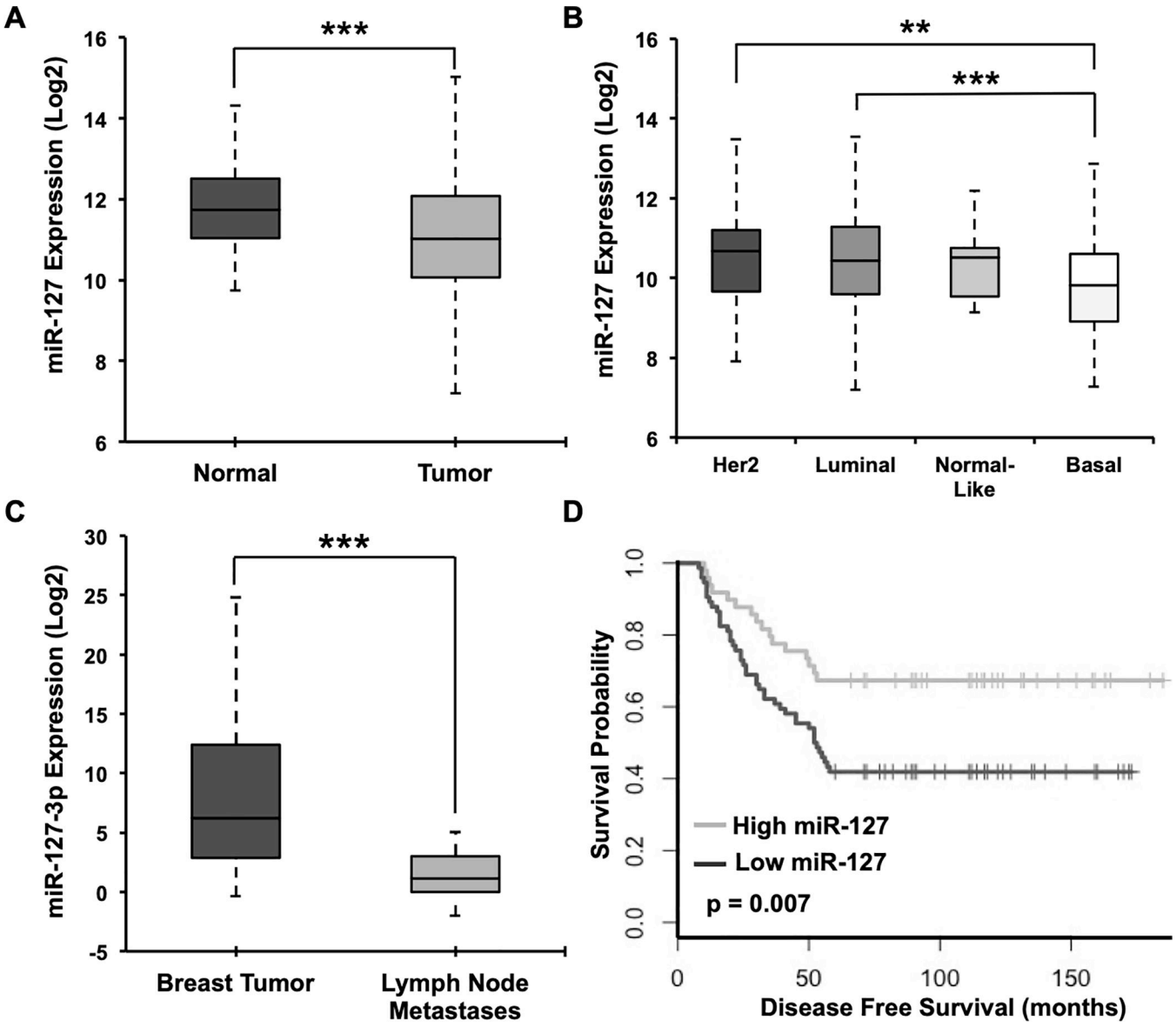

Figure 1. miR-127 in human breast cancer.

(A) Boxplot depicting expression levels of miR-127 in normal (n=103) and breast tumor (n=1101) samples. (Data from TCGA BRCA) **(B)** Boxplot depicting expression levels of miR-127 in Her2+ (n=57), luminal (n=349), normal-like (n=8), and basal (n=93) breast tumors. (Data from TCGA BRCA) **(C)** Boxplot depicting miR-127 expression in primary tumors (n=31) and lymph node metastases (n=13) of triple negative breast tumors. (Data from GSE38167) **(D)** Kaplan-Meier plot of disease-free survival as a function of miR-127 expression. Patients were segregated into two groups (High: n=49, Low: n=74) based on the expression status of miR-127 in their primary tumors using data driven cut-offs. (Data from GSE59829) ** and *** indicate $p < 0.01$ and $p < 0.001$, respectively.

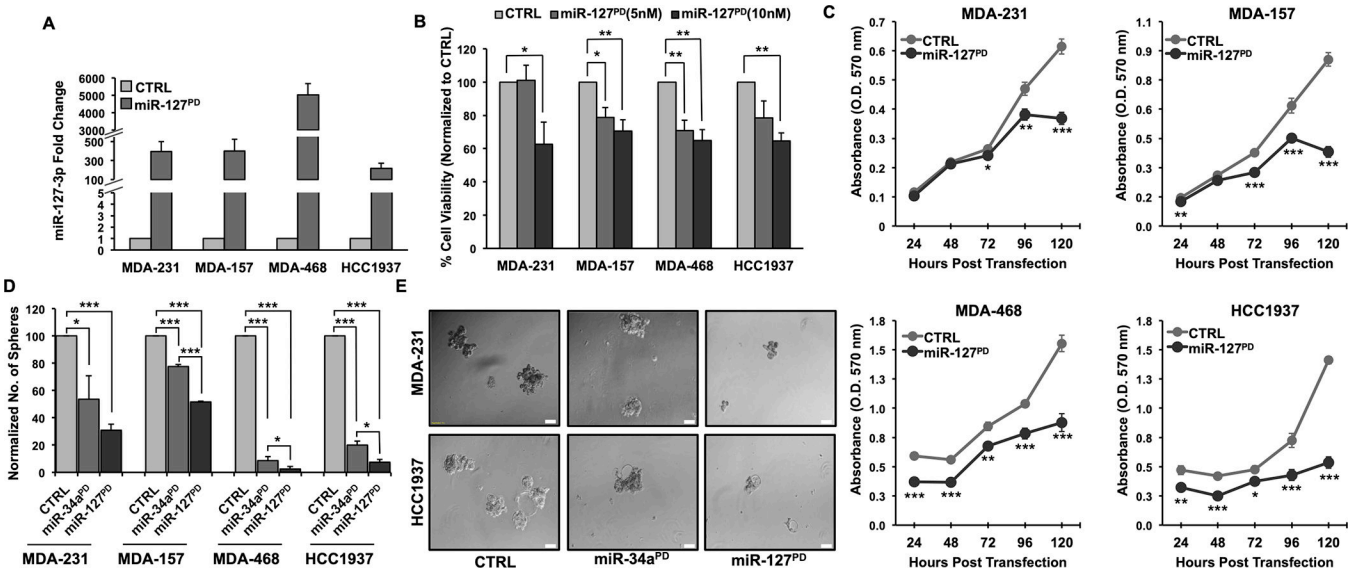

Figure 2. Impact of miR-127^{PD} expression on TNBC cell viability.

(A) Bar plot showing relative mature miR-127-3p expression levels in cells transfected with CTRL or miR-127^{PD}. Expression was determined from the Ct values using the $2^{-\Delta\Delta Ct}$ method after normalization to U6. **(B)** Bar plot of cell viability in four TNBC cell lines transfected with CTRL or miR-127^{PD}. Percent cell viability was determined after normalizing to CTRL values. CTRL values are set to 100%. **(C)** Impact of CTRL or miR-127^{PD} expression on cell viability over 5 days. **(D)** Impact of CTRL or miR-127^{PD} expression on tumorsphere formation. Bar plot showing normalized number of tumorspheres per 2500 cells. Tumorsphere counts were normalized to CTRL values, which are set to 100%. **(E)** Representative images of tumorspheres (bright field, 10X magnification, scale bar (white) is 50 μm). All values are mean ± S.E.M. of at least three biological replicates. *, **, and *** indicate $p < 0.05$, $p < 0.01$, and $p < 0.001$, respectively.

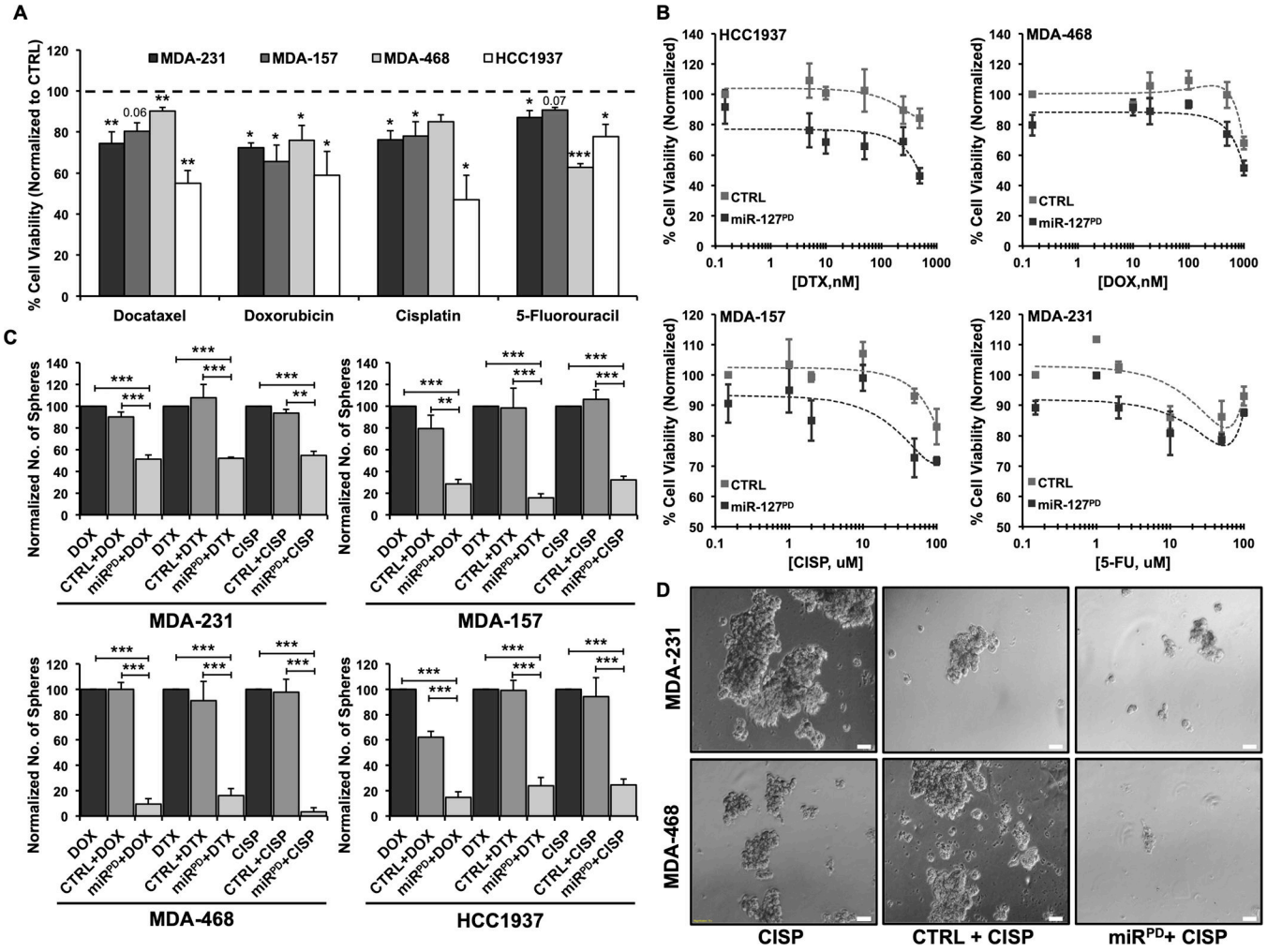

Figure 3. Impact of miR-127^{PD} expression on the chemosensitivity of TNBC cells.

(A) Bar plot showing percent cell viability in TNBC cell lines treated with either CTRL or miR-127^{PD} and chemotherapeutics (500nM Docataxel, 1uM Doxorubicin, 50uM Cisplatin, 2uM 5-Fluoruracil). Percent cell viability was determined after normalizing to CTRL values. CTRL values are set to 100% (dashed line). **(B)** Representative dose response curves of TNBC cell lines expressing CTRL or miR-127^{PD}. DTX (Docataxel), DOX (Doxorubicin), CISP (Cisplatin), and 5-FU (5-Fluoruracil). Percent cell viability was determined after normalizing to CTRL values with no drug added. CTRL values with no drug are set to 100%. **(C)** Impact of CTRL or miR-127^{PD} expression on cancer stem cell sensitivity to chemotherapeutics. Bar plot showing normalized number of tumorspheres per 5000 cells. Number of tumorsphere was determined after normalizing to "drug alone" (DOX, DTX, CISP) values. Drug alone values are set to 100%. **(D)** Representative images of tumorspheres (bright field, 10X magnification, scale bar (white) is 50 μm). Values are mean ± S.E.M. of three **(A)** and two **(B-C)** biological replicates. *, **, and *** indicate $p < 0.05$, $p < 0.01$, and $p < 0.001$, respectively.

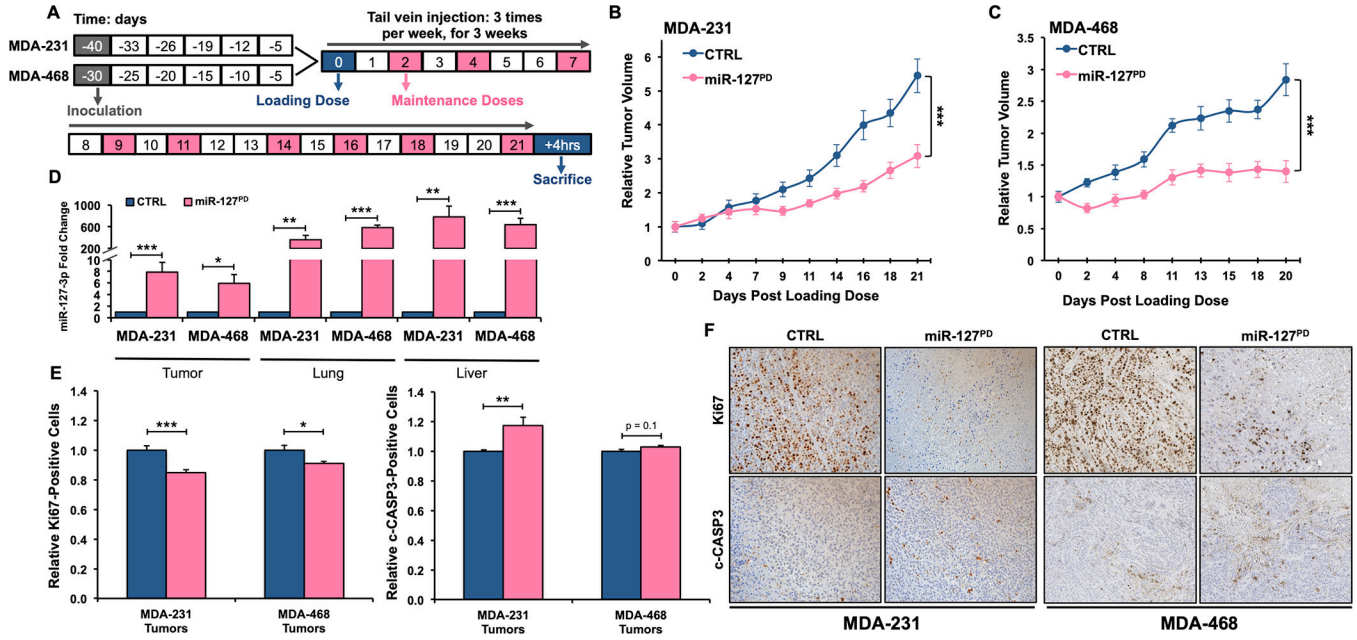

Figure 4. Impact of miR-127^{PD} expression on *in vivo* growth of MDA-MB-231 and MDA-MB-468 cells.

(A) Schematic depicting timeline of miR-127 *in vivo* experiment. **(B)** Line graph showing relative **(C)** MDA-MB-231 and **(D)** MDA-MB-468 tumor growth in mice treated intravenously with 10 doses of CTRL (n=8 for MDA-MB-231, n=9 for MDA-MB-468) or miR-127^{PD} (n=10). Relative tumor volume was determined after normalizing to mean tumor volume, by group, at initial dose. **(D)** Bar plot showing relative mature miR-127-3p expression levels in tumor, lung, and livers of mice treated intravenously with CTRL (n=3–6) or miR-127^{PD} (n=3–6). Expression was determined from the Ct values using the $2^{-\Delta\Delta Ct}$ method after normalization to U6. **(E)** Impact of miR-127^{PD} on tumor cell proliferation and apoptosis. Bar plots showing percentage of positive Ki67 and cleaved Caspase-3 cells in tumors of CTRL (n=4 for MDA-MB-231, n=8 for MDA-MB-468) and miR-127^{PD} (n=3–4 for MDA-MB-231, n=8 for MDA-MB-468) treated mice. Five random 20X fields were quantified per animal. Number of positive cells was determined after normalizing to CTRL values. CTRL values are set to 1. **(F)** Representative IHC images of Ki67 and cleaved Caspase-3 staining in tumors of CTRL and miR-127^{PD} treated mice. Values are mean ± S.E.M. *, **, and *** indicate $p < 0.05$, $p < 0.01$, and $p < 0.001$, respectively.

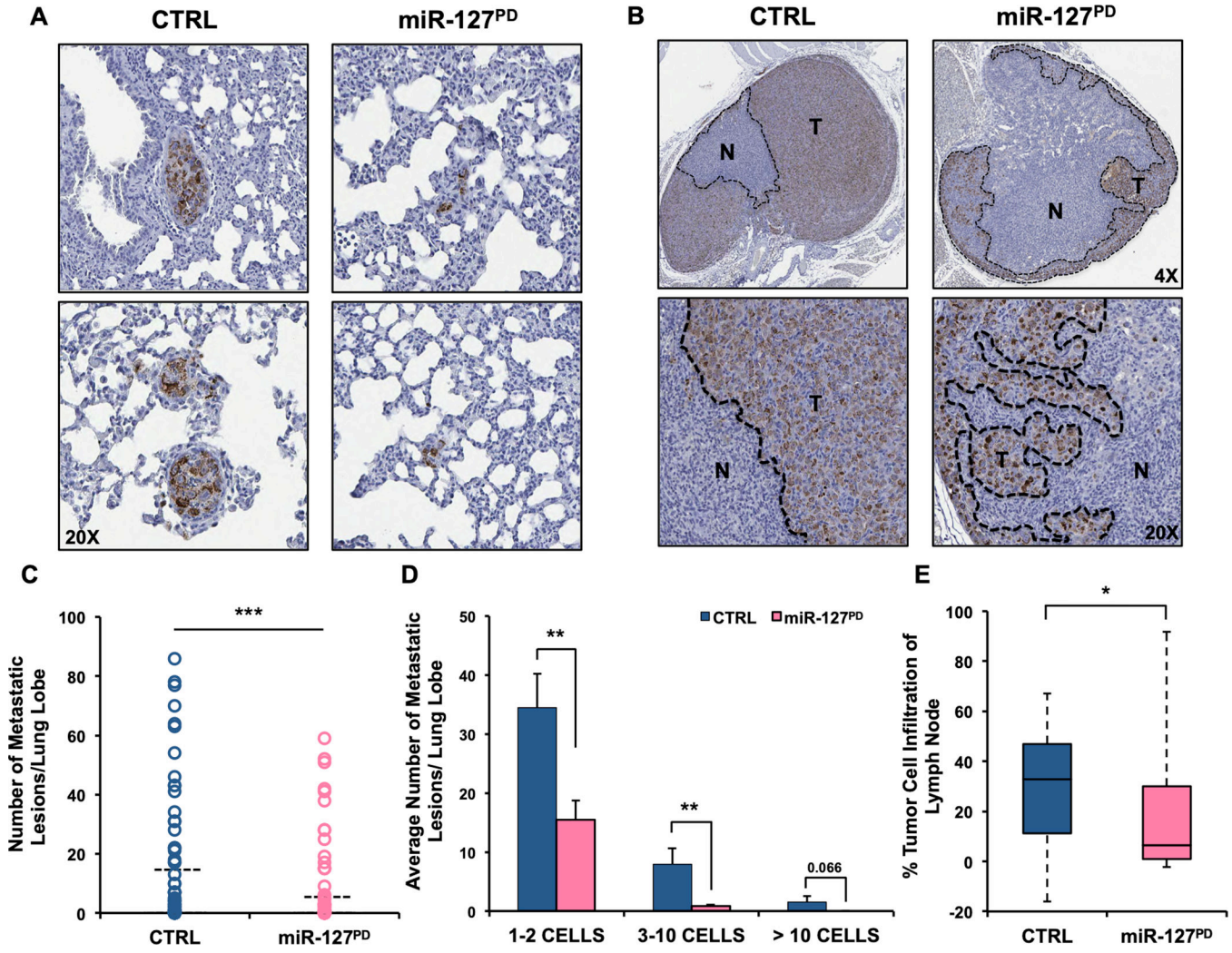

Figure 5. Impact of miR-127^{PD} expression on spontaneous metastasis of MDA-MB-231 cells.

(A) Representative IHC images (20X) of human-specific anti-mitochondrial antibody staining in the lungs of CTRL (n=7) and miR-127^{PD} (n=8) treated mice. **(B)** Dot plot depicting the total number of metastatic lesions in each lung section analyzed (CTRL, n=23 sections and miR-127^{PD}, n=31 sections). **(C)** Bar plot showing the average number of metastatic lesions in lungs stratified by colony size. **(D)** Representative IHC images (4X and 20X) of human-specific anti-mitochondrial antibody staining in the lymph node of CTRL (n=7) and miR-127^{PD} (n=8) treated mice. N = normal lymph node, T = MDA-MB-231 tumor cells. Dashed lines delineate the areas comprised of normal or tumor cells. **(E)** Boxplot showing the percent area occupied by MDA-MB-231 cells in the lymph node. Values are mean ± S.E.M. *, **, and *** indicate $p < 0.05$, $p < 0.01$, and $p < 0.001$, respectively.

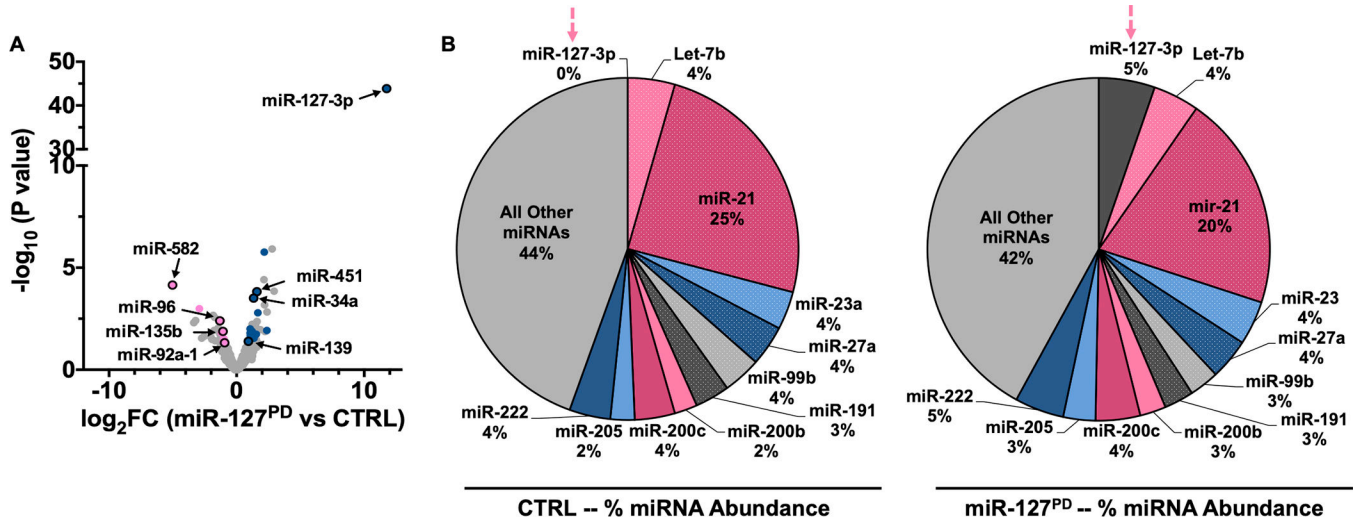

Figure 6. Analysis of miR-127-regulated miRNome.

(A) Small RNA sequencing analysis revealed differentially expressed miRNAs in miR-127^{PD} versus CTRL treated MDA-468 cells. Volcano plot showing differentially expressed sRNA and miRNAs. Significantly upregulated (blue) or downregulated (pink) miRNAs had 20%, or greater, increase or decrease, respectively, compared to CTRL, P-value < 0.05, and CPM > 5. **(B)** Pie charts showing percent abundance of miRNAs in CTRL (left) and miR-127^{PD} (right) small RNA sequencing samples. The change in abundance of miR-127-3p is indicated by pink arrows above pie charts.

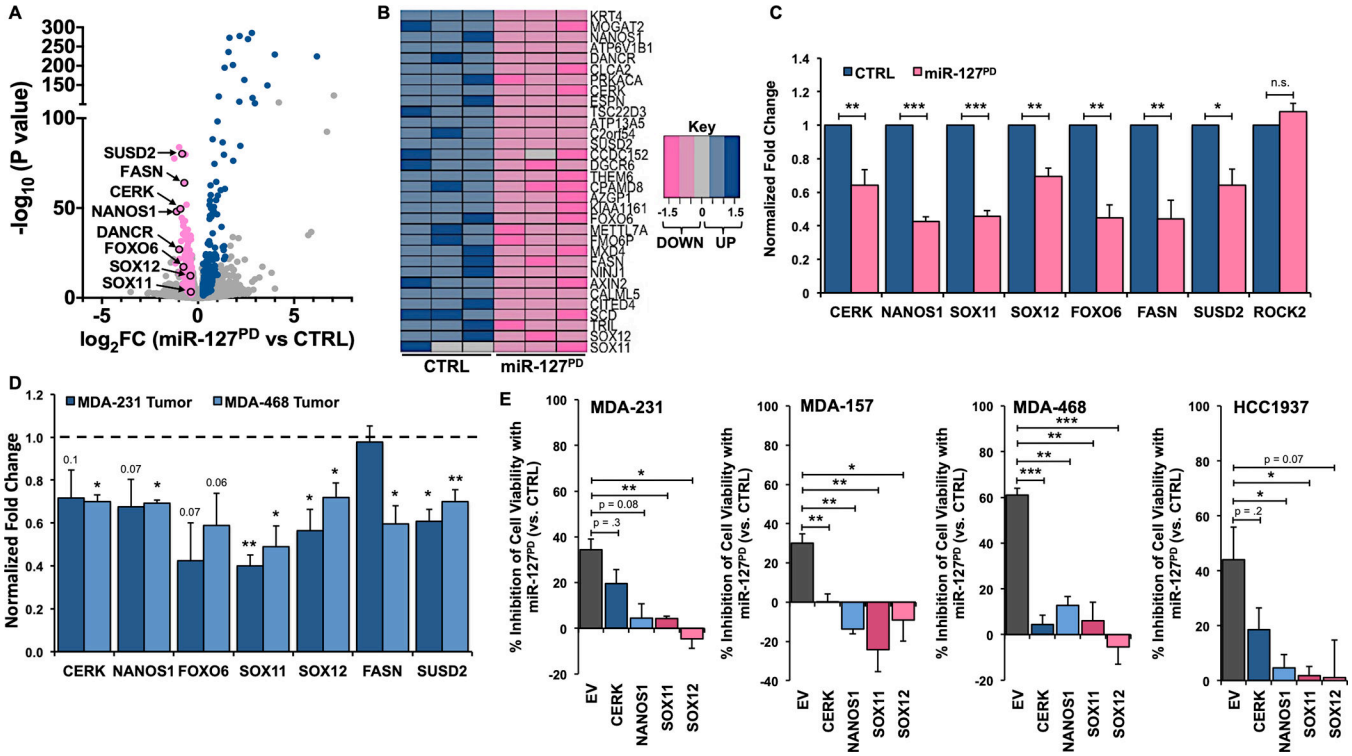

Figure 7. Genome-wide analysis of miR-127 by RNA Sequencing.

(A) RNA sequencing analysis revealed differentially expressed mRNAs in miR-127^{PD} versus CTRL treated MDA-468 cells. Volcano plot showing differentially expressed transcripts. Significantly upregulated (blue) or downregulated (pink) mRNAs had 20%, or greater, increase or decrease, respectively, compared to CTRL, P-value < 0.05, and CPM > 5. **(B)** Heatmap of the top 10% most downregulated transcripts in across three replicates of MDA-468 cells treated with miR-127^{PD} compared to CTRL treatment. **(C)** Bar plot showing relative expression levels of putative miR-127-3p targets in MDA-468 cells transfected with CTRL or miR-127^{PD}. (Note no change in miR-127-5p target, ROCK2). Expression was determined from the Ct values using the $2^{-\Delta\Delta Ct}$ method after normalization to GAPDH. **(D)** Bar plot showing relative expression levels of putative miR-127-3p targets in MDA-231 and MDA-468 tumors from mice systemically treated with CTRL (n=3) or miR-127^{PD} (n=3). **(E)** Bar plot of percent inhibition of cell viability in MDA-231, MDA-157, MDA-468, and HCC1937 cells co-transfected with CTRL or miR-127^{PD} and EV, CERK, NANOS1, SOX11, or SOX12 plasmid DNA. Percent inhibition of cell viability was determined after normalizing to CTRL values for each plasmid. Values are mean ± S.E.M. *, **, and *** indicate $p < 0.05$, $p < 0.01$, and $p < 0.001$, respectively.